Pluto's Spectrum from 1.0 to 4.2 μm: Implications for Surface Properties[1,2]

C. B. Olkin, E. F. Young, L. A. Young

Southwest Research Institute, Department of Space Studies, 1050 Walnut St., Boulder, CO

80302

W. Grundy[3]

Lowell Observatory, 1400 W. Mars Hill Road, Flagstaff, AZ 86001

B. Schmitt

Laboratoire de Planétologie de Grenoble, CNRS-UJF, Université J. Fourier, Bâtiment D de

Physique, B.P. 53, Grenoble cedex 9, 38041 France

A. Tokunaga, T. Owen

Institute for Astronomy, University of Hawaii, 2680 Woodlawn Drive, Honolulu, HI 96822

T. Roush

NASA Ames Research Center, MS 245-3, Moffett Field, CA 94035

and

H. Terada

Subaru Telescope, National Astronomical Observatory of Japan, 650 North A'ohoku Place,

Hilo, HI 96720

colkin@boulder.swri.edu

Received   _____ ;   accepted _____

ABSTRACT

We present spectra of Pluto's anti-Charon hemisphere obtained from the Keck and Subaru telescopes from 2.8 to 4.2 μm. Combined with 1 - 2.5 μm spectra from the IRTF telescope, this collective data set lets us constrain several surface frost properties. The surface area of pure nitrogen frost (as opposed to nitrogen with dissolved methane) is constrained to be 6% or less. The ratio of pure to dilute (in nitrogen) methane frost is best fit by a ratio of 3 to 4. The grain size of pure methane is constrained to be near 200 μm. We were not able to constrain the temperature of pure methane. An additional surface component with spectral properties similar to 'Titan tholin' was necessary to fit the entire 1 to 4.2 μm spectrum; our best-fit model requires 21% of Pluto's anti-Charon hemisphere (by area) to be this Titan-tholin component. Contrary to Sasaki et al.'s (2005) spectra of Pluto's sub-Charon hemisphere, we find no evidence for other hydrocarbons in the 3-3.3 μm region.

Subject headings: planets and satellites: Pluto

1.   Introduction

Previous spectral studies of Pluto have identified surface constituents and various properties of surface frosts. We extend our knowledge of Pluto's surface frosts by simultaneously modeling data sets ranging from 1 - 4.2 μm.

The density of Pluto is very close to 2 gm/cm^3, suggesting that Pluto is a roughly 50/50 mixture of rock and water ice. H_2O is the major surface frost on Charon, but has not yet been convincingly detected on Pluto. In fact, only three surface frosts have been definitively identified on Pluto at present: N_2, CH_4 and CO. Methane has been separately identified in two forms, as pure CH_4 and dissolved in an N_2 matrix. Both CO and CH_4 are trace components in the N_2 matrix, but CH_4 is so optically active that it dominates Pluto's spectrum (Douté et al. 1999). Nitrogen has been identified from a weak 2.148 μm feature. The shape of this feature is temperature dependent and has been used to constrain the N_2 frost temperature to 40 ± 2 K (Tryka et al. 1994). Douté et al. (1999) point out that the nitrogen band shape is indicative of β N_2, but that extracting the nitrogen temperature requires a thorough modeling of the underlying CH_4 band shape. Also, Grundy et al. (2002) point out that deriving a temperature from a single band is hazardous.

Like Triton (whose N_2 atmosphere was detected by Voyager (Nelson et al. 1990)), Pluto's atmosphere is sustained by the vapor pressure of N_2 frost. This vapor pressure is an extremely steep function of temperature, and as a result, the N_2 frost temperature is nearly uniform over Pluto's entire surface despite large latitudinal variations in insolation. The sunnier parts of Pluto are cooled by sublimating N_2 frost while less illuminated regions are warmed by condensation. If the N_2 frost temperature were to increase by one and a half degrees, the atmospheric pressure would double. Even small increases in the temperature of Pluto's sunlit N_2 frosts would produce unsustainable pressure gradients, but a quantitative definition of "small" is still and outstanding question, one that is a key part of volatile

transport models.

CO is 3-5 times less volatile than N_2, and CH_4 is 5 orders of magnitude less volatile(Brown & Ziegler 1980). CH_4 has been detected in Pluto's atmosphere (Young et al. 1997) with a tentative identification of CO (Bockelée-Morvan et al. 2001). The presence of gas-phase CH_4 implies a source on Pluto's surface, which in turn suggests the presence of pure CH_4 hot spots at temperatures around 55 K, the temperature at which CH_4's vapor pressure is equal to that of N_2 at 40K. Previous lab work has shown that 3.3 and 7.8 μm bands of CH_4 are effective thermometers (Ngoh et al. 1993).

In practice, the 3.3 μm ν_3 methane band on Pluto is saturated to the point where we have little sensitivity to the CH_4 temperature. However, this wavelength range is effective at constraining the areal abundance of nitrogen frost and the relative areal coverage of pure methane vs. methane dissolved in nitrogen.

2. Observations and Data Reduction

We present spectra from two instruments, NIRSPEC (McLean et al. 1998) and IRCS (Kobayashi et al. 2000), mounted on the Keck II and Subaru telescopes, respectively. The NIRSPEC spectrum ranges from 2.8 to 3.6 microns, while the IRCS spectrum extends further to 4.2 microns. Neither instrument was operated with adaptive optics. The NIRSPEC observations took place on August 12, 2001 with the KL filter, while the Subaru observations took place about a year later July 23, 2002 at nearly the same Pluto longitude (Table 1). The NIRSPEC slit width was 42x0.380 arcsec, corresponding to a resolution of R $\approx$ 4000. The IRCS slit was 0.3 arcsec wide (5.2 pixels), for a resolution of R $\approx$ 350-500.

[Table 1: List of Observations and Associated Geometry]

2.1.   Reduction of Keck observations

First, we discuss the reduction of the NIRSPEC observations. We derived the wavelength calibration from images of a Neon lamp. We fit a quadratic polynomial to seven lines identified across the image with a residuals to the fit of less than 0.002 microns.

The A-B flattened spectral image pairs (of the standard star spectrum and Pluto-Charon) were rectified then had a column-by-column background subtraction applied to remove as much residual sky counts as possible at each wavelength by sampling the background above and below the rectified trace, robustly fitting a line to those samples (omitting outliers), and subtracting the fitted line from that column. We used optimum extraction (Horne 1986) to improve SNR over aperture extraction and allow identification of outliers.

The Pluto-Charon observations were interleaved with observations of the nearby solar analog star BS6060 (Porto de Mello et al. 1997). The standard star observations bracket the airmass of the Pluto-Charon observations (1.2 to 1.4 airmasses). For each Pluto-Charon observation, we constructed a solar analog spectrum corresponding to the airmass of Pluto. Each Pluto-Charon spectrum was normalized by the extinction-corrected solar analog spectrum to remove the telluric and solar contributions.

The resulting spectrum is the mean of 37 individual observations. The mean spectrum was binned in wavelength by 10 pixels. Each individual Pluto spectrum included 20 coadds each with an integration time of 3 seconds. The ensemble spectrum has an effective exposure time of 37 minutes.

We have written an IDL pipeline to accomplish these tasks. The IDL routines and documentation are available online at "www.boulder.swri.edu/~colkin/nirspec04/Pluto3um/ Reduction_Method_V2.htm".

2.2. Reduction of Subaru observations

For the Subaru observations, we followed the same basic method for extracting the Pluto-Charon spectrum from the data when possible. Lamp images were not available for these observations, so we used atmospheric lines to determine the wavelength calibration. These lines were identified from synthetic telluric transmission plots generated with ATRAN (Lord 1992).

We flattened the images (Akiyama et al. 2002) and removed the column-by-column background signal from the A-B pairs. We used observations of the solar analog star HR8883 to remove the telluric and solar contributions from Subaru observations. This star was observed at one visit during the night with a mean airmass of 1.47 compared to a mean airmass of 1.27 for the Pluto observations. With the standard star spectra only available at a single elevation, we cannot fit an empirical airmass versus extinction function. In principle, we could use a tool like ATRAN to model the transmission of the terrestrial atmosphere at an airmass of 1.47 and 1.27 and make corrections to the standard star spectrum. In practice this correction did not make a significant difference to the HD8883 spectrum.

[Figure 1, Pluto spectrum]

3. Analysis

We generate synthetic spectra of Pluto for a broad range of possible surface properties using Hapke theory Hapke (1993). In Section 4.4, we discuss sensitivity tests which indicate where changes in parameters affect synthetic spectra most strongly and we point out spectral regions that constrain specific surface properties such as pure N_2 abundance and methane grain size.

We use Hapke's equivalent-slab approximation to calculate the scattering efficiency from the optical constants of the assumed surface ices. We have developed IDL routines based on Hapke theory to derive the bi-directional reflectance for a single-layer or two-layer surface including the effects of surface roughness. From Hapke (1993), we have the following equation for the bidirectional reflectance:

$$r_R(i, e, g) = \frac{w}{4\pi} \frac{\mu_{0e}}{\mu_{0e} + \mu_e}[[1 + B(g)]p(g) + H(\mu_{0e})H(\mu_e) - 1]S(i, e, g) \tag{1}$$

where w is single-scattering albedo. The cosine of the incidence angle and emission angle, commonly presented as μ_0 and μ, have additional terms to account for the tilt of the surface (due to surface roughness) and become μ_{0e} and μ_e, respectively. The function $B(g)$ accounts for the opposition effect.

$$B(g) = \frac{B_0}{1 + \frac{1}{h}tan\frac{g}{2}} \tag{2}$$

The constant B_0 is the ratio of the light scattered from the face of the particle near the Sun to the total amount of light scattered at zero phase. The other term of the opposition effect is an approximation to the exact formula for the fall off of flux with phase angle, g due to the opposition affect. We have assumed a value for the compaction parameter, h, of 0.5. Parametric studies have shown the model spectra to be insensitive to this parameter over its whole range of possible values (0 to 1). The Chandrasekhar's H-function is computed using Hapke's (1993) approximation.

The function S(i,e,g) is the shadowing function and accounts for shadows cast on one part of the surface by another and surfaces that are preferentially tilted toward the source or detector.

We have assume a Henyey-Greenstein (?) phase function

$$p(g) = \frac{B_0}{1 + \frac{1}{h}2\xi cos(g) + \xi^2} \tag{3}$$

where ξ is the cosine asymmetry factor.

For a 30x30 grid across the projection of Pluto in the plane of the sky we compute the incident and emission angle from each surface element. Using the viewing geometry for each surface element on Pluto, we compute the bidirectional reflectance. The geometric albedo is the ratio of the brightness of a body at a phase angle of zero to the brightness of a perfect Lambert disk of the same radius and distance from the Sun observed and illuminated normally. We have made no corrections to our data or model to account for the small (non-zero) phase angle of these observations, see Table 1. Pluto has not been observed at phase angles of zero yet. This will have to wait until 2018 (?) when Pluto passes through the ecliptic plane. All of these observations have a phase angle between 1.2 and 1.8 degrees and the model spectra have been computed for a phase angle of 1.76 °.

The geometric albedo is the sum over all the Pluto surface elements of the product of the bidirectional reflectance and the cosine of the emission angle times pi over the number of surface elements.

For a single composition terrain, we use the formalism described above directly. To model multiple geographical terrain units on Pluto, the geometric albedo spectra of the individual components are summed with weights equal to the fractional area of each terrain. To model an intimate mixture (often referred to as a salt-and-pepper mixture) of different compositions, we need modify the parameters of the particles that enter the bidirectional reflectance equation (Hapke, 1993). Specifically, the single-scattering albedo becomes the single-scattering albedo of the average weighted by cross-sectional area. Similarly, the opposition effect term, B_0, is also the weighted average of the individual B_0's. The cross-sectional area is the fractional volume divided by the size of the grains, following

Grundy (Grundy 1995).

We have considered surface terrain units composed of pure CH_4, CH_4 diluted in N_2, N_2, H_2O, and two types of tholins. We also considered intimate mixtures of CH_4 and tholin and found that only a small fraction of tholin will mask the spectral features of CH_4. We were able to investigate temperature dependencies for the pure CH_4 and CH_4 diluted in N_2 because the optical constants as a function of temperature were available (Table 2). We used optical constants from Grundy et al. (2002) for CH_4 as a function of temperature (spanning 30K to 90K), from B. Schmitt (personal communication) for CH_4 diluted in N_2 as a function of temperature over the range 36.5K to 43K. The H_2O ice optical constants were combined from two sources (Grundy & Schmitt 1998), (Trotta 1996) to cover the wavelength range from 1.0 to 4.2 μm. These two sources of H_2O optical constants only overlap in temperature at 60K. We consider two tholin compositions. One was produced from an initial gas mixture rich in CH_4 (Khare et al. 1984) and the other from a mixture more rich in N_2 (Khare, personal communication; described in more detail in Cruikshank et al. (2005)).

[Table 2: List of Optical Constants]

The free parameters in our model are the cosine asymmetry parameter, ξ, the grain sizes of each surface terrain, temperatures of CH_4 and CH_4 dissolved in N_2, the concentration of CH_4 in N_2, the fractional coverage of each surface terrain type on the Earth-facing hemisphere of Pluto, surface roughness, and the compaction parameter. We have modeled a range of asymmetry parameters from forward scattering to isotropic to backscattering. This parameter largely affects the albedo level of the continuum regions of the spectrum, as can be seen in Figure **??**. A backscattering asymmetry parameter improves the fit between the synthetic spectrum and the observations by increasing the continuum level between methane bands. For this reason, we limit the models considered from here on

to values of ξ equal to -0.3 which is near the global value found for Triton from Voyager (Hillier et al. 1994). Parametric studies have shown that varying the surface roughness, an input to the S(i,e,g) function and the μ_{0e} and μ_e functions, does not significantly affect the synthetic spectrum. We have assume a surface roughness of 14 degrees based on analogy to Triton (Hillier et al. 1994).

We generated more than 5000 model spectra covering a broad range of parameter space. The details of the parameter space considered for single-layer terrains are given in Table 3. Many of the models were two-layer models (combining pure and dilute CH_4) and covered much of the same parameter space as the single-layer models.

[Table 3: List of Parameters]

We have used previous spectrophotometric observations of (Spencer et al. 1990) (at 2.9 μm) to convert the reflectance spectrum of Pluto-Charon to geometric albedo (due to slit loss). The passband of the (Spencer et al. 1990) data extends shortward of the NIRSPEC data, so we fit a line to the NIRSPEC data and scaled it such that the albedo at the center of the passband matched the value of the (Spencer et al. 1990) spectrophotometry. The spectrophotometric data were recorded over many (5) nights and therefore, do not correspond to single sub-Earth longitude and latitude. Nonetheless, they are the best albedo data in this wavelength range.

The NIRSPEC slit was oriented along the Pluto-Charon line. Since the disk of both Pluto and Charon are within the slit, the relative contributions of each is simply their fractional areas to the total. Charon composes 20% of the area of the combined disks of Pluto and Charon given that Pluto's radius is approximately twice Charon's. The albedo difference between Charon and Pluto is included in the model spectra. We model the Charon spectrum with pure H_2O ice darkened to have an albedo that matches the geometric albedo of Charon around 1.8 microns (Buie & Grundy 2000). The Charon model is reduced

by the fractional area of the whole (20%) and is removed from the observed spectrum of Pluto and Charon (see Figure 2). There are not published models of Charon-only spectra in the 3-micron region, therefore, we assume the same model of darkened H_2O ice that dominates Charon's spectrum at the shorter wavelengths (Buie & Grundy 2000) is dominant at 3 microns.

[Figure 2, Charon model]

Spectra of typical individual components are shown in Figure 3 . The shift of the CH_4 band centers for a concentration of 0.36% CH_4 diluted in N_2 is seen by comparison of the blue and the green curves.

[Figure 3, showing individual components]

4.   Results

4.1.   Comparison with Previous Surface Models

The best spectroscopic models published to date are those of Douté et al. (1999) that fit observations one face of Pluto's surface from 1.4 to 2.6 microns. Coincidentally, these data correspond to nearly the same sub-Earth longitude as the Douté et al. (1999) data. Douté et al. (1999) found three models that fit the observations well. We have extended the Douté et al. (1999) models out to 4.2 μm (see Figure **??**) and observe that none of the three models are consistent with the longer wavelength spectra. All three models show excess flux around the ν_3 band of CH_4 from 3.1-3.6 μm.

Each of the Douté et al. (1999) models is composed of 3 geographical terrains which are combinations of pure methane, methane diluted in nitrogen and pure nitrogen. All three models have 12% of Pluto's surface covered with fine-grained pure nitrogen frost.

Nitrogen frost is bright, but not very optically active in this region with only one weak, but important, band at 2.148 microns. The overall effect of adding a terrain unit of pure nitrogen is to increase the albedo of the surface across all wavelengths from 1 to 4.2 microns. The increase of signal at 3 microns is not consistent with the data.

[Figure 4, Doute models at 3 microns]

Also of interest in Figure 4 is the slope of the observed spectrum from 2.9 to 3.2 microns when compared to the models of Douté et al. (1999). This edge of the 3.3 methane ice absoprtion features is sensitive to the relative amounts of pure methane versus methane that is dissolved in nitrogen ice. Our best-fit model has a pure to dilute methane ratio of near 1:1. One of the Douté et al. (1999) models has similar proportions and this model best fits the 2.9 to 3.2 micron region.

The very low albedo around the ν_3 band of CH_4 from 3.1-3.6 μm constrains the fraction of pure N_2 on Pluto's surface. Pluto's spectrum observed from Keck in the 3-4 μm range constrains the anti-Charon hemisphere of Pluto's surface to have less than 6% pure N_2 by area, see Figure 5 and Figure 6. This upper limit is only on the areal fraction of PURE nitrogen and does not limit the amount of nitrogen in solid solution with methane or in an intimate mixture with a darker component such as tholins (more on this in Section 5).

[Figure 5, nitrogen limits based on Keck data]

[Figure 6, nitrogen limits based on Subaru data]

4.2. Evidence for Tholins

In this section we continue the search for surface consistuents that will fit Pluto's spectrum from 1.0 to 4.0 microns. We initially considered combinations of pure methane,

methane diluted in nitrogen and pure nitrogen. We considered geographical mixtures of these components singly and in combination (i.e. layered terrains or intimate mixtures). We searched a large space of different parameters (described previously, see Table 3) and were unable to match the observed spectrum with only these three ices because of the albedo difference at the depths of the 2.4 and 3.3 μm methane features. No combination of these three units would match the observations. Another compositional unit with less absorption at 2.3 μm than at 3.3 μm is required.

We investigated the affects of adding small-grain H_2O ice and two different tholins. All three of these components have less absorption at 2.35 microns than 3.3 microns, see Figure 3. However, only the "titan" tholin (Khare et al. 1984) provided a good fit. The other components both had an increase in albedo near 3.6 μm that was not matched in the data. This is not definitive evidence for tholin on Pluto's surface particularly since we are not matching distinctive spectral bands. However, the observations indicate that something with a spectral signature consistent with Khare (1984) tholin exists on Pluto's surface.

Since we often consider Triton as an analog of Pluto, one might wonder why the Titan tholin provided a better match than the triton tholin to the observations. This is less surprising when one considers the relative amounts of methane on the surfaces of Pluto and Triton. Pluto is more rich in methane than Triton and the so-called Titan tholin mixture differs from the Triton tholin mixture in that it is produced from more methane rich precursors. We stress that the name "Titan tholin" has nothing to do with substances observed on Titan or on Pluto; it is simply a convenient name for a laboratory-produced substance that has optical properties that improved our model fit.

We investigated the possibility of hiding significant amounts of pure nitrogen in the tholin terrain unit as an intimate mixture. Much like a small amount of dirt will significantly reduce the reflectance of snow on Earth, a small amount of tholin in an intimate mixture

with nitrogen will take on the spectral signature of the darker material (tholin, in this case). Less than 5% tholin imtimately mixed in a nitrogen ice matrix will produce a spectrum that is indistinguishable from the tholin itself.

4.3. Our Best-Fit Model

Using the tools described in the previous section to generate synthetic spectra, we started with single-layer, single-component terrain units to find a model that fits the observations well. This was accomplished with a three-terrain unit model (Figure 7) consisting of 21% Khare et al. (1984) tholin with 10 μm grains, 37% CH_4 at 60K with 200 μm grains, and 42% CH_4 diluted in N_2 at 41K with 95 cm "grains" (more on this later), see Figures 8 and 9. The concentration of CH_4 in N_2 is 0.36 %. This model may not be unique in its goodness-of-fit and relies on the assumptions inherent in the Hapke formalism as well as the surface components considered. Nonetheless, this model and its sensitivities provide insight into the surface of Pluto. There are some spectral regions that are diagnostic of surface features.

[Figure 7, Pie chart showing best fit model]

[Figure 8, Best Fit Model short wavelengths]

[Figure 9, Best Fit Model long wavelengths]

4.4. Sensitivity Studies

This work was motivated by a desire to determine the temperature and grain size of the pure methane frost on Pluto's surface. Unfortunately, the 2.8 to 4.0 micron spectra are not sensitive to the methane temperature, but they can provide a good estimate of the

methane grain size. We carried out sensitivity studies of all our model parameters about our best-fit solution.

Increasing the CH_4 grain size changes the amplitude of the peaks of the methane features around 1.70 and 2.23 microns. Figure 10 shows the effect of changing the methane grain size from our nominal model. The shorter wavelength methane features 1.1 to 1.3 μm have less of a dependance on this parameter.

[Figure 10, Changes in pure methane grain size]

The slope of Pluto's spectrum from 2.8 to 3.1 μm is diagnostic of the ratio of the areas of pure to dilute CH_4. As seen in Figure 3, the pure CH_4 ice has a steeper slope than the dilute CH_4. The effect of varying the geographic fraction of CH_4 to N_2:CH_4 is shown in Figure 11.

Another way to assess the sensitivity of our models is to look at the derivative of the model spectrum with respect to each of the parameters. Figures **??** to **??** show the derivative for each of the free parameters in the model about the best-fit model discussed above. Comparison of the figures shows a significant correlation between the cosine asymmetry parameter, grain sizes of pure and dilute CH_4 and the concentration of methane in N_2 from 2.9 to 3.7 μm. This is because all of these act to increase the path-length of light through CH_4 ice.

There are some differences. The asymmetry factor also controls continuum level. Backscattering particles are consistent with our best Pluto analog (Triton) and they also help to increase the albedo of the model spectrum. If we chose an isotropic scattering function, then we would need to have smaller grain sizes in the tholin terrain to increase the over-all brightness of the synthetic spectrum. This is possible, but then the grain size of the tholin is approaching the wavelength of the light and we are in a different regime for

modeling the reflectance.

[Insert Figure 12 here, Derivative figures.]

4.5.   Evidence for other hydrocarbons

Sasaki et al. (2005) have proposed that there are non-methane hydrcarbons on Pluto's surface from spectra in this 3-micron region taken at Subaru with the same instrument and AO. Our observations do not require the presence of higher-order hydrocarbons; they are well fit by our model with pure methane, methane diluted in nitrogen and tholin. We fit the inflection points of Pluto's spectrum in the region of 3.1 to 3.3 microns without additional hydrocarbons. Note, however, that the Sasaki et al. (2005) spectrum is different from our Subaru spectrum and it is difficult to assess the significance of this without error bars on the Sasaki et al. (2005) data. The explanation may be that the non-methane hydrocarbons on Pluto's surface are preferentially located on the hemisphere observed by Sasaki et al. (2005) which is about 145 degree away from our observations, see Figure 13.

[Insert Figure 13 here, Pluto map]

Pluto's surface composition is regionally variable. The anti-Charon hemisphere that we observed in this work features higher average albedos along with more nitrogen and CO ice absorption and lower daytime temperatures (Lellouch et al. 2000; Grundy and Buie 2001). In contrast, Pluto's sub-Charon hemisphere shows much less nitrogen and CO absorption, and stronger absorption by the weakest methane bands, indicative of highly concentrated methane ice deposits. The fraction of CH_4 ice I versus CH_4 diluted in nitrogen also varies strongly with longitude, being much higher on the sub-Charon hemisphere. Additionally, the continuum regions of Pluto's infrared spectrum exhibit considerable regional variation (Grundy and Buie 2002). The nitrogen-rich areas which dominate the longitudes we

observed show relatively little continuum absorption compared with other regions. The CH$_4$-rich regions on Pluto's other side show continuum absorption more like Triton analog tholin (Khare et al. 1994) unlike the Titan analog tholin we favor in the models presented here. Completely different continuum absorption behavior is seen around the longitude of minimum light in Pluto's visible wavelength lightcurve. In those regions, a mixture of water ice and Titan tholin offers a good match to spectral observations (Grundy and Buie 2002).

5. Discussion

One of the most striking results from the analysis of spectra longward of 2.5 μm is the upper limit on the areal fraction of pure N$_2$ ice. Large amounts of N$_2$ frost must be present of Pluto's surface, based on the strength of the weak 2.148 μm nitrogen feature, but virtually none of that N$_2$ frost is free of contaminants.

Pluto's surface must experience massive resurfacing over the course of a Pluto year (248 years). Pluto's heliocentric distance in 1989 (perihelion) was just under 30 AU, and its aphelion distance will be ∼50 AU. Pluto's subsolar latitude is close to zero at perihelion and aphelion, but its obliquity is nearly 90deg (i.e., Pluto rotates on its side). As a result, large regions of Pluto's surface experience decades of permanent sunlight or darkness. As thin as it is, Pluto's atmosphere thought to be sufficient to support the transport of volatiles from warm to cold regions of the surface. (Contrast this situation to that of Io, whose atmosphere is so thin that cryo-volanic volatiles from a local plume that only resurfaces the satellite in the neighborhood of the source.)

If Pluto's atmosphere freezes out to the point that winds emanating from the subsolar point would have to exceed the speed of sound to reach the antisolar point before condensing on the surface, then Pluto too would lose its global atmosphere. At present, however,

occultation observations show that Pluto's atmosphere is global and has, in fact, doubled in column abundance from 1988 to 2002 (Sicardy et al. 2002; Elliot et al. 2002).

Consider what would happen to a region of Pluto's surface as it moves into permanent darkness. The condition for condensation onto the surface requires that a gas's partial pressure exceed the vapor pressure of that constituent in the surface frost. If one assumes that actual surface pressure is essentially that same as the vapor pressure of N_2 frost (a compelling assumption, given that N_2 frost is the most volatile surface species), then CH_4 molecules in the atmosphere will begin to condense onto the surface well in advance of N_2 molecules, *unless* the molar abundance of CH_4 gas is so low that the CH_4 partial pressure is lower than CH_4 frost's vapor pressure.

Methane gas has been detected in Pluto's atmosphere at the few percent level (L. Young et al), a level that far exceeds the equilibrium level expected for CH_4 based on the ratios of N_2 to CH_4 vapor pressures. A common assumption to explain the atmospheric CH_4 excess is that there must be CH_4 hotspots on Pluto's surface that supply methane to Pluto's atmosphere. In any case, it is reasonable to assume that CH_4 molecules are present over Pluto surface at levels that exceed the equilibrium value (i.e., the vapor pressure of CH_4 mixed in N_2 ice is probably less than the partial pressure of CH_4 in the atmosphere). As long as this is the case, then it would be difficult for N_2 ice to form *without* entrained CH_4 ice.

The implication of the low (6 percent by area) upper limit on pure N_2 frost is that methane gas is always available in the atmosphere whenever and wherever N_2 frost is condensing. This could be a result of long diffusion and circulation timescales in Pluto's atmosphere, which might make it impossible for *all* of the CH_4 to condense onto Pluto's surface before the N_2 gas begins to condense, but virtually nothing is known about the circulation of Pluto's atmosphere. Another possible source for methane would be sunlit

hotspots that manage to supply CH_4 gas to the dark side, even as Pluto's global atmosphere begins to freeze out as Pluto approaches aphelion. Again, the details of Pluto's seasonal circulation patterns will be needed to resolve how easily gas-phase CH_4 is transported around Pluto's globe. Our hope is that the observed limits on pure N_2 frost will constrain future circulation models.

The grain size of methane diluted in N_2 is best fit by extremely large sizes of 95 cm. Grain sizes of 50 cm and smaller are inconsistent with Pluto's 3.3 micron spectral feature; the smaller grain sizes produce a spectral feature that is narrower than the observed spectrum. In the past, the strength of the 2.148 μm nitrogen band has implied very large grain sizes for nitrogen ice diluted with methane (Ref). We do not use the 2.148 μm band to constrain our surface frost model, but the width of the 3.3 μm band forces us to accept very large grain sizes for the N_2 with dissolved CH_4. "Grain size" may be better throught of as "path length" at these sizes, but regardless of terminology, the scattering centers in N_2 with dilute CH_4 seem to be well separated. This independent evidence for large grain sizes implies a mechanism for annealing N_2 frost into a relatively pristine ice. Eluscewiecz (200X) suggests that the large grain sizes are an artifact of the Hapke formalism, and that the actual distance between scattering centers may be less than 95 cm (check this).

The pure methane grain sizes are best fit with a diameter of 200 μm, significantly smaller than the N_2-CH_4 mixture. The pure methane grain sizes are constrained in the same way as the CH_4 diluted in N_2, by the width of the 3.3 μm feature. Grain sizes of 100 microns or smaller produce synthetic spectra that are too narrow in the 3.3 micron band, and grain sizes of 400 μm produce model spectra that are too wide. The grain sizes of the pure vs. dilute methane ice are so different that they prompt the question: can we separate the relative abundances of the two forms of CH_4 from their grain sizes?

The relative abundances of pure vs. dilute CH_4 are well determined from two

independent pieces of Pluto's spectrum. First, the line centers of methane bands (at 2.2 to 2.4 microns) depend on whether CH_4 is pure or dissolved in N_2 frost. Second, the slope of the spectrum from 2.9 to 3.2 μm is sensitive to the ratio of pure vs. dissolved methane. The spectrum of pure methane has a steeper slope in this region.

Now we address questions having to do with the formation and processing of tholins. The general production mechanism is thought to be a loss of H-atoms from CH_4 or longer hydrocarbons due to incident UV photons or charged particles. On Pluto (unlike Triton), the current column abundance of CH_4 is sufficient to produce an atmospheric opacity of greater than one to Lyman-alpha photons; the opacity is due to the ionization cut-off of CH_4. In other words, UV photolysis of CH_4 is more important in Pluto's atmosphere than in the upper surface layers. However, charged particles do reach Pluto's surface, and these will produce complex nitrogen-hydrocarbon products from CH_4 diluted in N_2 ice (Moore and Hudson, 2003). One of the products found by Moore and Hudson (2003), diazomethane, may act as a catalyst to form long branched alkanes from CH_4. Diazomethane was also found by Bohn et al (1993) in experiments in which they irradiated N_2-CH_4 mixtures with UV light.

There seems to be ample laboratory evidence that either charged particles or UV photons should produce complex hydrocarbons on Pluto. These are collectively called "tholins," and they are much less volatile than frosts of N_2, CO or CH_4. If that is the case, then the relative areal abundances of tholin-rich terrain to tholin-free ices should constrain the seasonal rates of sublimation and condensation of N_2 frost. Young (PhD 1992) predicts that tens of centimeters of N_2 should sublimate from Pluto's sunlit hemisphere or condense on Pluto's shadowed hemisphere during a half-Pluto year. It should be easy to cover tholin-ruch terrain during a region's condensation phase, and tholins should accumulate on the surface during a region's sublimation phase. Even a minute fraction of tholin mixed

in with a bright frost will dramatically decrease the frost-and-tholin's albedo and increase that region's sublimation rate.

Two of the striking aspects of Pluto's albedo distribution are that (a) Pluto has very bright and very dark terrain, and often these units are adjacent to each other, and (b) the dark terrain on Pluto actually shows more color variation than the bright terrain (Young et al. 2001). This color variation is indirect evidence that several kinds of darkening agents exist. We found a single tholin whose optical constants let us match the observed spectrum of Pluto from 1 to 4.2 microns, but there are undoubtedly an array of darkening agents on Pluto, as evidenced by variation of continuum spectral characteristics with longitude (e.g., Grundy and Buie 2002).

A continuing question with respect to formation of tholins is the absence of ethane and acetelyne, the first products of irradiated methane. The report of hydrocarbons besides CH_4 by Sasaki et al. (2005) is intriguing because it represents the detection of the missing link between $N_2:CH_4$ and tholins. We note that the two Subaru spectra (ours and that of Sasaki et al.) look substantially different in the 3.0 - 3.3 μm region. These two spectra were obtained in May and July of 2002 (for the Sasaki et al. and our observations, respectively), only a few months apart, but at sub-Earth longitudes that differed by 145deg. More observations are called for over a greater range of Pluto rotational phases. For the moment we note that our Keck and Subaru spectra (both imaging Pluto's anti-Charon hemisphere) do not require other hydrocarbons to fit the 3.0 - 3.3 μm region.

6. Conclusions

We present a 3-terrain surface model that is consistent with observations from 1 to 4 microns of Pluto's anti-Charon face. Our best-fit model has 21% of the observed surface

covered with fine-grained titan tholin, 34% pure methane frost, and 42% of very dilute (0.36 %) methane in solid solution with nitrogen.

We are able to learn the following about Pluto's surface from this work: 1. Less than 6% of this hemisphere of Pluto's surface is covered with pure nitrogen. Although nitrogen may exist in significant amounts as an intimate mixture with tholin and not be spectroscopically visible at these wavelengths. 2. There is evidence for titan tholin (or something spectroscopically similar) on Pluto's surface from the albedo differences between the shorter wavelength methane bands and the 3-micron methane band. 3. The fraction of pure to dilute methane is well constrained near 1:1 by the slope of Pluto's spectrum from 2.8 to 3.2 microns. 3. The grain size of the pure methane is 200 plus-or-minus 100 microns. 4. There is no evidence for other hydrocarbons on this face of Pluto.

Facilities: Keck:II, IRTF (SpeX), Subaru.

REFERENCES

Akiyama, M., Ueda, Y. & Ohta, K. 2002, The Astrophyical Journal, 567, 42.

Bockelée-Morvan, D., Lellouch, E., Biver, N., Paubert, G., Bauer, J., Colom, P. & Lis, D. C. 2001, A&A, 377, 343.

Brown, G. N., Jr., & Ziegler, W. T. 1980, Adv. Cryog. Eng., 25, 662.

Buie, M. W. & Grundy, W. M. 2000, Icarus, 148, 324.

Cruikshank, D. P., Owen, T. C., Ore, C. D., Geballe, T. R., Roush, T. L., DeBergh, C., Sandford, S. A., Poulet, F., Benedix, G. & Emery, J. P. 2005, Icarus, 175, 268.

Douté, S., Schmitt, B., Quirico, E., Owen, T. C., Cruikshank, D. P., de Bergh C., Geballe, T. R., Roush, T. L. 1999, Icarus, 142, 421.

Grundy, W.M., B. Schmitt & E. Quirico 1993, Icarus, 105, 254.

Grundy, W.M. 1995, Ph. D. thesis, U of A.

Grundy, W.M. & B. Schmitt 1998, J. Geophys. Res. 103, 25809.

Grundy, W. M., Buie, M. W., Stansberry, J. A. & Spencer, J. R. 1999, Icarus, 142, 536.

Grundy, W. M. & Buie, M. W. 2001, Icarus, 153, 248.

Grundy, W. M. & Buie, M. W. 2002, Icarus, 157, 128.

Grundy, W. M., Schmitt, B., & Quirico, E. 2002, Icarus, 155, 486

Hapke, B. 1993, Theory of Reflectance and Emittance Spectroscopy, Cambridge Univ. Press, New York.

Horne, K. 1986, Pub. Astron. Soc. Pacific 98, 609.

Hillier, J., J. Veverka, P. Helfenstein, & P. Lee 1994, Icarus, 109, 296.

Kobayashi, N., Tokunaga, A. T., Terada, H., Goto, M., Weber, M., Potter, R., Onaka, P. M., Ching, G. K., Young, T. T., Fletcher, K., Neil, D., Robertson, L., Cook, D., Imanishi, M. & Warren, D. W. 2000, SPIE, 4008, 1056.

Khare, B. N., Sagan, C., Arakawa, E. T., Suits, F., Callcot, T. A. & Williams, M. W. 1984, Icarus, 60, 127.

Lellouch, E., R. Laureijs, B. Schmitt, E. Quirico, C. de Bergh, J. Crovisier & A. Coustenis 2000. Icarus 147, 220.

Lord, S. D. 1992. NASA Technical Memorandum 103957.

McLean, I. S., Becklin, E. E., Bendiksen, O., Brims, G., Canfield, J., Figer, D. F., Graham, J. R., Hare, J., Lacayanga, F., Larkin, J. E., Larson, S. B., Levenson, N., Magnone, N., Teplitz, H. & Wong, W. 1998, SPIE, 3354, 566.

Nelson, R. M., Smythe, W., D., Wallis, B. D., Horn, L. J., Lane, A. L., & Mayo, M. J. 1990, Science, 250, 429.

Ngoh, M. A., Khanna, R. K. & Fox, K. 1993, JGR, 98, 5511.

Owen, T.C., T.L. Roush, D.P. Cruikshank, J.L. Elliot, L.A. Young,C. de Bergh, B. Schmitt, T.R. Geballe, R.H. Brown & M.J. Bartholomew 1993. Science 261, 745.

Porto de Mello, G. F. & L. da Silva 1997. Astrophysical Journal Letters 482, L89.

Sasaki, T., Kanno, A., Ishiguro, M., Kinoshita, D. & Nakamura, R. 2005, The Astrophysical Journal, 618, L57.

Spencer, J. R., Buie, M. W., & Bjoraker, G. L. 1990, Icarus, 88, 491.

Trotta , F. 1996. Ph.D. dissertation at Universite Joseph Fourier.

Tryka, K. A., Brown, R. H., Cruikshank, D. P., Owen, T. C., Geballe T. R. & De Bergh, C. 1994, Icarus, 112, 513.

Young, L. A., Elliot, J. L., Tokunaga, A., de Bergh, C. & Owen T. 1997, Icarus, 127, 258.
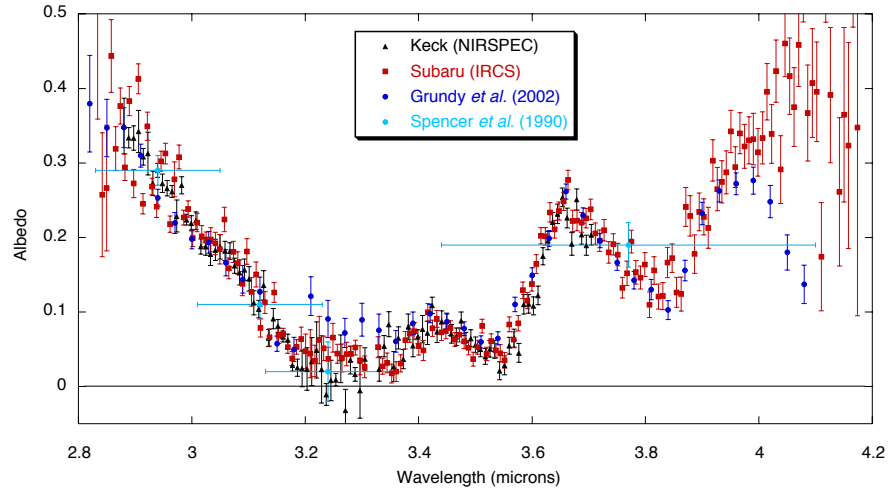

Fig. 1.— Keck-NIRSPEC observations previously published data in this wavelength range. The Keck and Subaru spectra were normalized to the spectrophotometry data point at 2.9 μm from (Spencer et al. 1990).
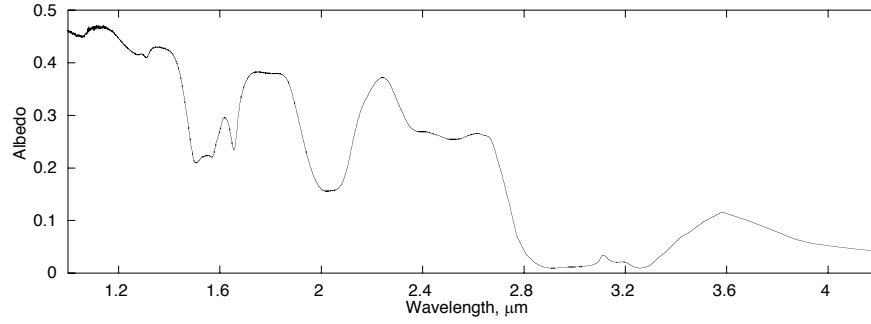
This manuscript was prepared with the AAS LaTeX macros v5.2.

Fig. 2.— A model of Charon's spectrum in the range of our observations. We are assuming a darkened water ice model matching the observations of Buie & Grundy (2000). Beyond 2.5 microns there is no published spectrum of Charon, but we assume the darkened water ice model continues out to 4.2 microns. We used optical constants from Grundy and Schmitt (1998) to model the spectrum out to 2.7 microns and data from Trotta (1996) for the optical constants from 2.7 to 4.2 microns.
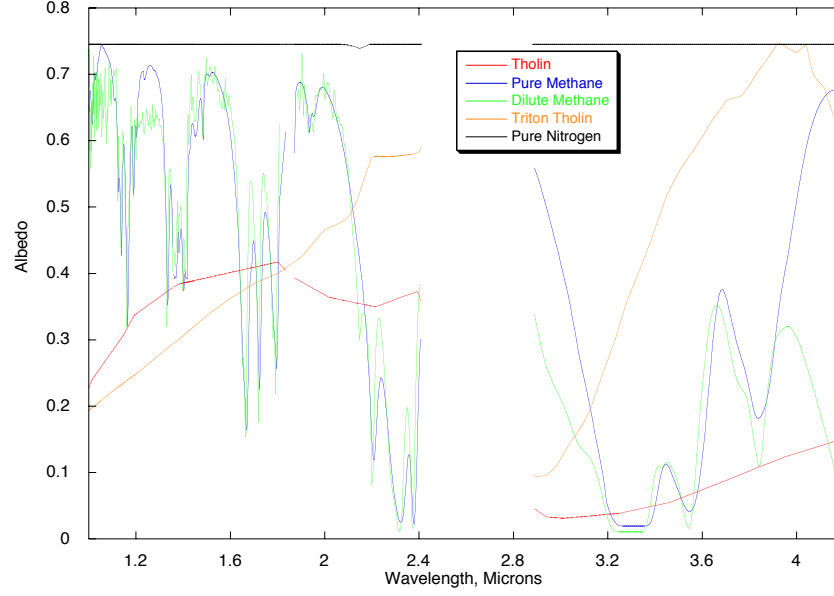
Fig. 3.— The spectra of typical individual components considered. We considered pure methane (blue), methane diluted in nitrogen (green), two different types of tholins (Titan tholin is red and Triton tholin is orange) and pure nitrogen (black).
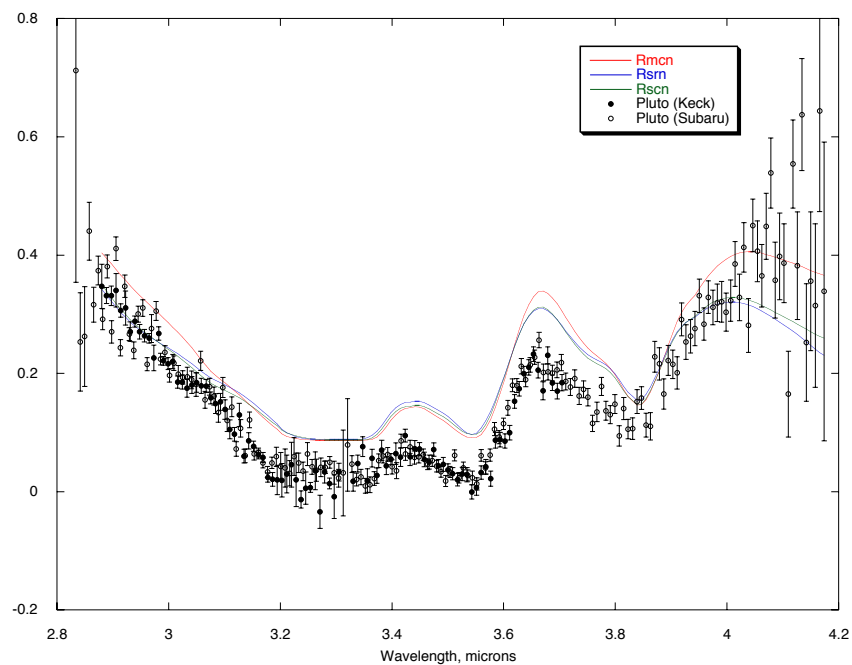
Fig. 4.— The models of Doute et al. (1999) evaluated at 2.8 to 4.2 microns with the observations in this wavelength range. The Keck data are represented with solid circles and the Subaru are open circles.
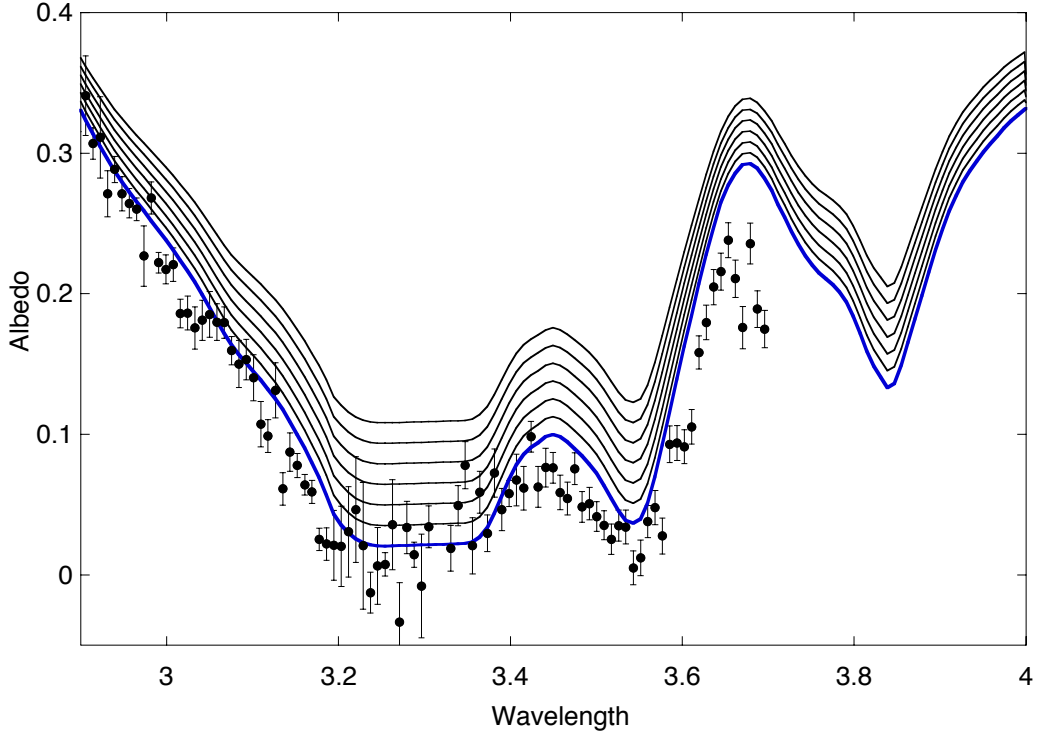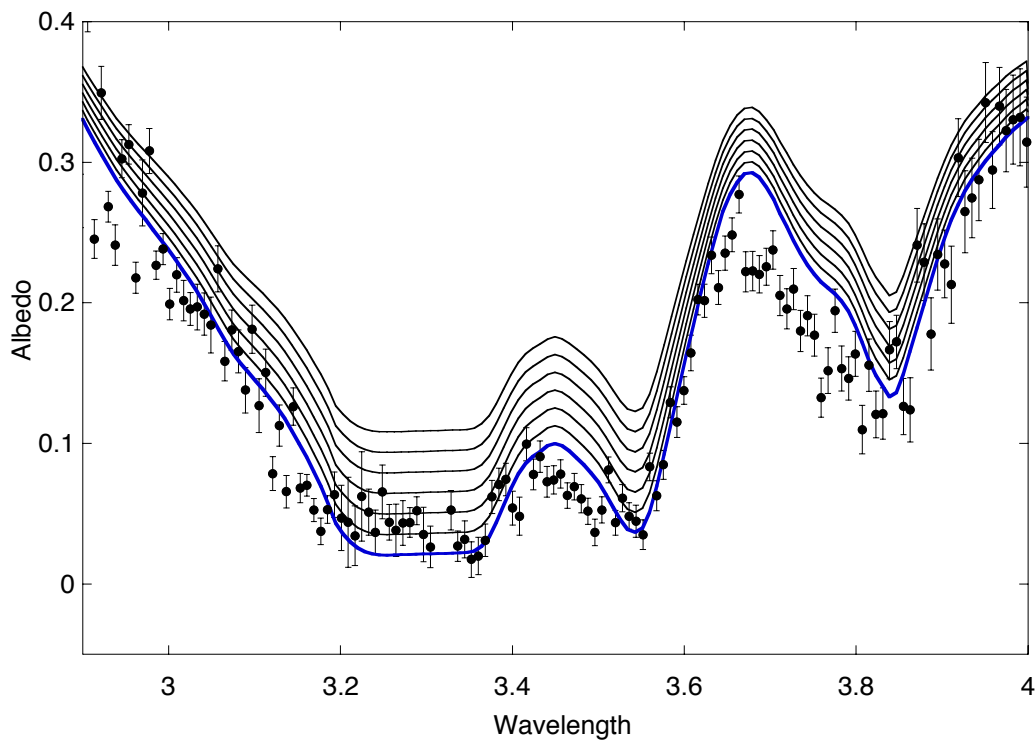
Fig. 5.— Pluto spectrum from Keck observations and models. The best-fitting model is the thick line. The other lines include from 2 to 12 % N_2 by steps of 2%. From 3.2 to 3.4 microns, we can see that the data are inconsistent with the larger fractional areas of pure N_2.

Fig. 6.— Pluto spectrum from Subaru observations and models. The best-fitting model is the thick line. The other lines include from 2 to 12 % N$_2$ by steps of 2%. From 3.2 to 3.4 microns, we can see that the data may accomodate 2-4 % pure N$_2$ but not 8-12%.
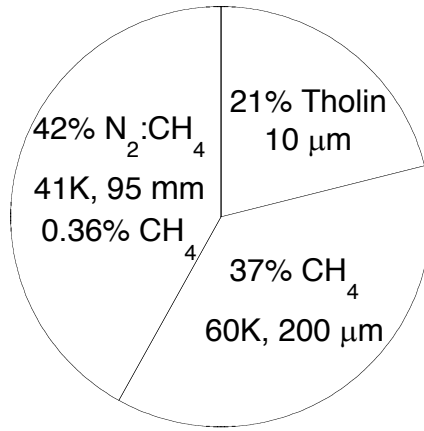
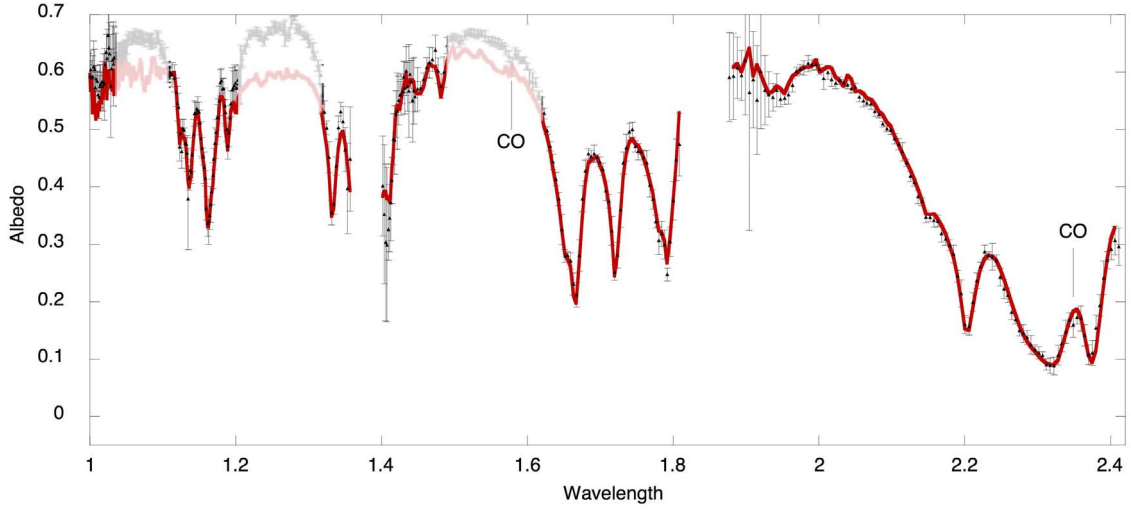Fig. 7.— A pie chart of the geographical terrain units in our best-fit model.

Fig. 8.— The observations (black) and best-fitting model (red) over the wavelength range of 1 to 2.4 microns. The difference between model and data in the continuum regions near 1.1, 1.3 and 1.5 microns are not significant. These areas have been de-emphasized in this figure. It is difficult to calibrate the optical constants for the dilute methane in these regions where there is little absorption. Also evident are two CO features, previously identified by Doute et al. (1999), at 1.579 microns and 2.354 microns. These were not modeled in our synthetic spectra (red line).
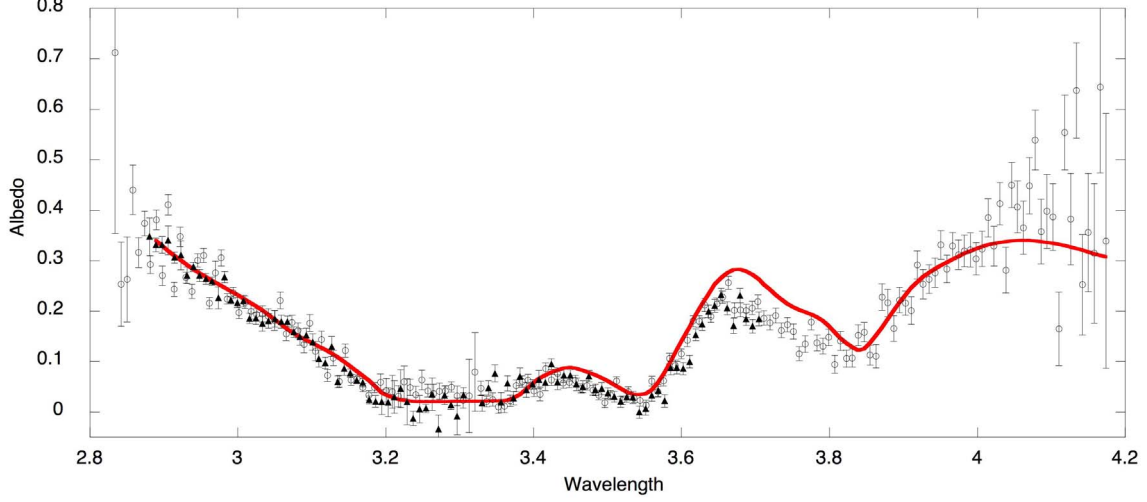
Fig. 9.— The observations (black) and best-fitting model (red) over the wavelength range of 2.8 to 4.2 microns. The slope from 2.8 to 3.2 microns is an indicator of the relative amount of pure and dilute methane on Pluto's surface. The depth of the 3.3 micron features is well matched by our best-fitting model which has no pure nitrogen frost.
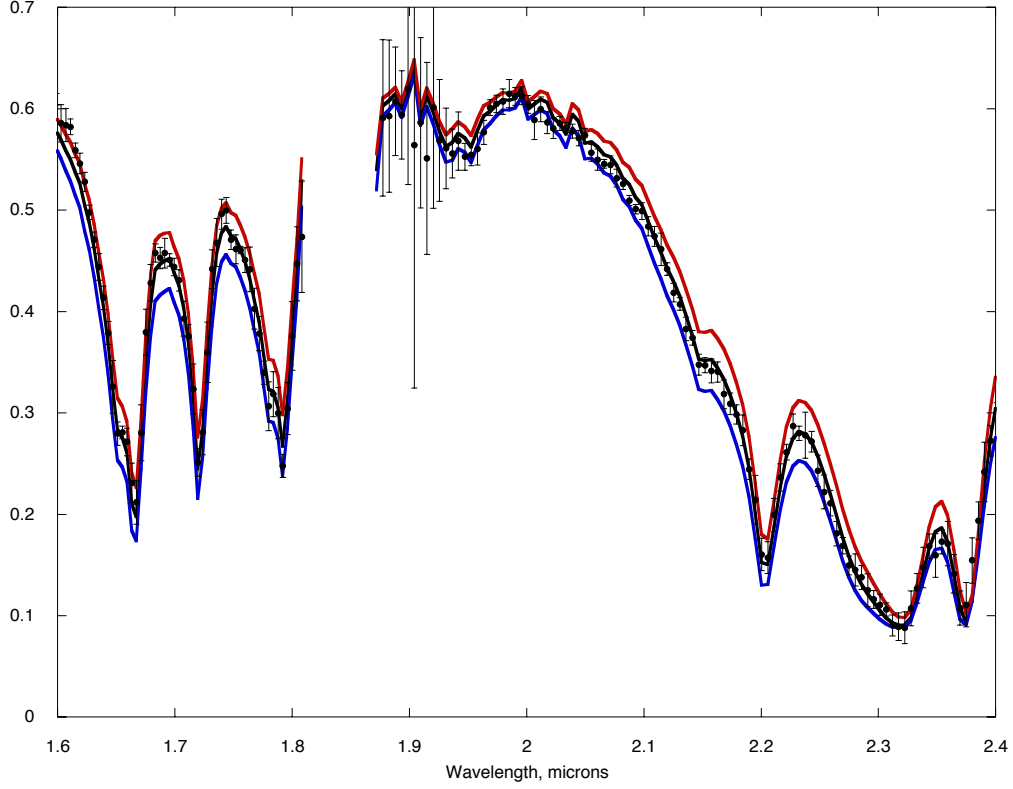
Fig. 10.— The sensitivity of the methane features near 2 microns to changes in the pure CH_4 grain size. The data are from Keck; the black line is the best-fit model. The blue and red curves are variations of the best fit model. The blue line is the best-fit model with 400 micron grains for the pure methane terrain unit and the red line is the best-fit model with 100 micron grains for the pure methane terrain unit.
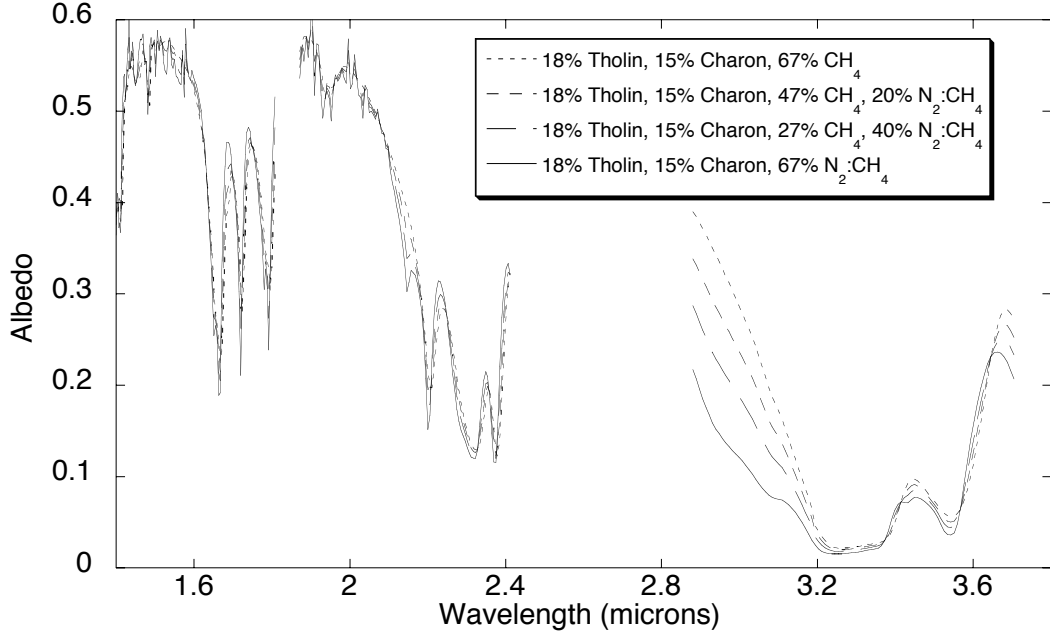
Fig. 11.— The effect on spectral models of varying the fraction of pure and dilute methane. All models contain 18% tholin and 15% Charon contribution. The remaining 67% is varied from all CH_4 (shot-dashed line) to CH_4 diluted in N_2 (solid line). The most significant differences are the slope of the spectrum from 2.9 to 3.2 μm and at the 2.14 μm N_2 band.
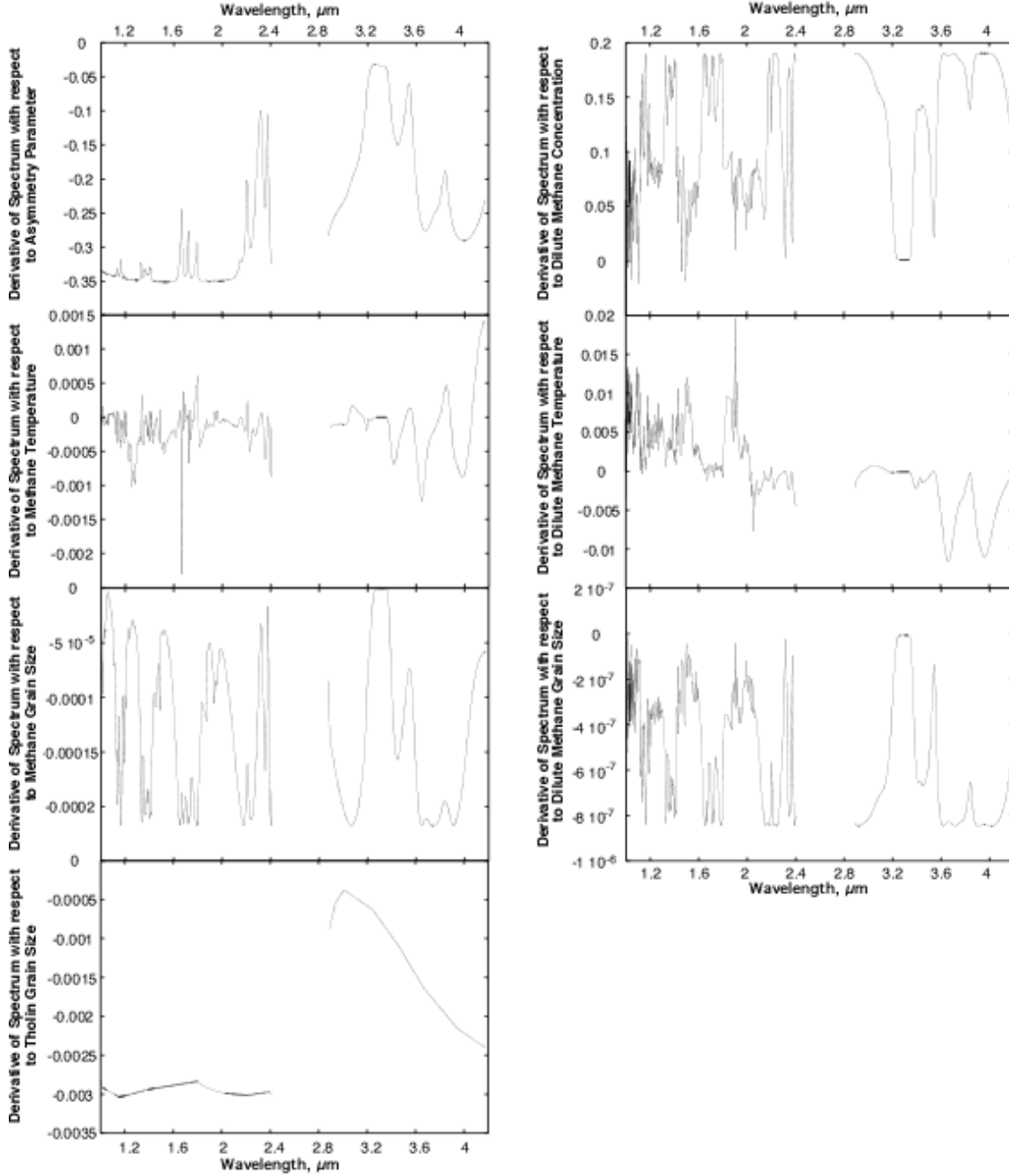
Fig. 12.— The derivatives of the Pluto spectrum with respect to the model parameters. If the derivatives of two parameters are correlated or anti-correlated at all wavelengths, then those two parameters can not be separated. For example, the derivatives of dilute methane grain size, dilute methane concentration and the asymmetry parameter are all correlated (or anti-correlated) in the 3-4 micron range. The magnitude of the derivatives indicates how tightly we can constrain a parameter. For example, dilute methane grain size has small variations in its derivative. Hence we can only constrain this parameter on millimeter scales.
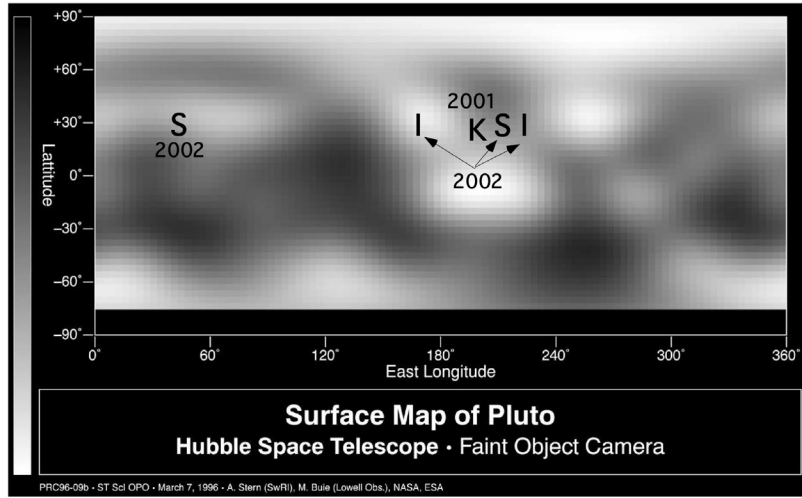
Fig. 13.— A map of Pluto's surface showing the sub-Earth points on Pluto during each of the observations. The Keck observations are indicated with a "K", the Subaru Telescope observations presented in this paper are the "S" near the center of the map, and IRTF observations are indicated with an "I". The "S" located near 45 degrees east longitude indicates the viewing geometry during the Sasaki et al. (ref) observations from Subaru in 2002.

Table 1. Observational Circumstances

Telescope	Instr.	Date	λ (μm)	Res. (raw)	Res. (binned)	Sub-⊕ Pluto long.	Sub-⊕ Pluto lat.	Phase Angle
IRTF	SpeX	Jul. 16, 2002	0.8-2.4	4200	420	170°	-29°	1.22°
IRTF	SpeX	Jul. 17, 2002	0.8-2.4	4200	420	226°	-29°	1.24°
Keck II	NIRSPEC	Aug. 12, 2001	2.9-3.7	4000	400	198°	-26°	1.76°
Subaru	IRCS	July 23, 2002	2.8-4.2	2000	400	207°	-28°	1.37°

Based on IAU definition of Pluto's north pole.

Table 2.   Optical Constants

Source	Composition	Wavelength Range	Temperature
Grundy et al. (1988)	H2O	0.96 - 2.74	20-270K by 10K
Trotta (1996)	H2O	2.5 - 17.4	15K, 60K
Grundy et al. (2002)	CH_4	0.65 - 4.91	20-90K by 10K
Schmitt (personal comm.)	N_2:CH_4	1.0 - 5.0	35K 36.5K, 38K, 41K, 43K
Schmitt (personal comm.)	N_2	1.0 - 5.0	35K 36.5K, 38K, 41K, 43K
Khare (1984)	Titan tholin	0.02 - 920.	
Khare (personal comm.)	Triton tholin	0.05 - 123.	

Table 3. Model Parameters Considered

Composition	Temperature	Grain Size	concentration	Asymmetry Parameter
CH_4	30, 40, 50, 60, 70	2, 50, 100, 200, 400, 500, 1000, 50000	-	-0.3, 0, 0.5
$N_2 : CH_4$	38, 41, 43	2, 500, 1k, 50k, 90k, 95k, 100k, 110k	0.25, 0.36, 0.5, 1, 2	-0.3, 0, 0.5
N_2	38, 41, 43	2, 5, 10, 50, 100, 200, 500, 750, 1000, 50k	-	-0.3, 0, 0.5
Titan Tholin	-	2, 5, 10, 50, 100, 200, 500, 750, 1000, 50k	-	-0.3, 0, 0.5
Triton Tholin	-	2, 5, 10, 50, 100, 200, 500, 750, 1000, 50k	-	-0.3, 0, 0.5